ESPI Measurement to Determine Interfacial Transition Zone in Cementitious Materials under Temperatures

Huang-Hsing Pan[1], Jhan-Cheng Li[1], Tsung-Chin Hou[1] and Kun-Sheng Liao[1]
[1]*Department of Civil Engineering, Kaohsiung University of Applied Sciences, Kaohsiung, Taiwan*
E-mail: pam@cc.kuas.edu.tw

ABSTRACT: Electronic speckle pattern interferometer (ESPI) is used to measure the micro-displacement of interfacial transition zone (ITZ) in cementitious materials under temperature fluctuations. The micro-displacement of ITZ is observed at top, bottom, left and right positions near a single aggregate, respectively. The maximum displacement of ITZ occurs at temperature 230°C to 330°C and depends on the observed position. Displacements of ITZ experience an inverse change as the applied temperature goes beyond 230°C. Out-of-plane displacement of ITZ with respect to the distance from the aggregate shows a more stable development than in-plane displacement at all temperatures. Based on ESPI measurements, a criterion to determine the ITZ is also presented. The ITZ at bottom position of an aggregate is about 80 μm evaluated from in-plane displacement and a slight difference from out-of-plane evaluation. Results indicate that ITZ can be determined by out-of-plane evaluation at temperature above 50°C.

1. INTRODUCTION

In microscopic view, cementitious materials can be considered as a three-phase composite consisting of binder, aggregates and interfacial transition zone (ITZ). Among those, interfacial transition zone is considered as the weak point that dominates the strength of concrete [1]. Many microscopic measurement techniques have been used to investigate the compositions and microscopic structure of ITZ, such as scanning electron microscopy (SEM) [2-6], backscattered electron images (BSE) [7], environmental scanning electron microscopy (ESEM) and optical microscopy (OM) [8-9]. Other instruments such as X-ray diffraction test [4,10], mercury intrusion porosimetry (MIP) [9,11] and micro-indentation test [5,12] were also chosen to investigate the material properties of ITZ. Most of them distinguish the realm of ITZ by exploiting image, the porous and loose characteristic in ITZ. Some researchers have also discussed the microstructural features, stress-strain relation and microcracks of ITZ at various temperatures [13-15].

In this study, we attempt to investigate the micro-displacement of ITZ in cementitious materials induced by the temperature from 30°C to 420°C. The composite specimens consist of cement mortar and single sand stone (coarse aggregate). Interfacial transition zone lies in between the mortar and the coarse aggregate. The displacement in ITZ was measured at the material age of 28 days by ESPI (electronic speckle pattern interferometer), a non-contacted measurement different from SEM. Determination of interfacial transition zone is also presented.

2. EXPERIMENTS

2.1 Materials

The mortar used in this study composed of Type I Portland cement with w/c=0.35 and 20% quartz sand with the particle size about 0.7-1.0mm and the specific gravity of 2.65. A 50×50×50mm specimen contains mortar matrix and a cylindrical sand stone (aggregate) with ϕ 10×15mm located at the center of the specimen, as shown in Fig.1. The specific gravity of the sand stone is 2.74 with absorption of 1.24%.

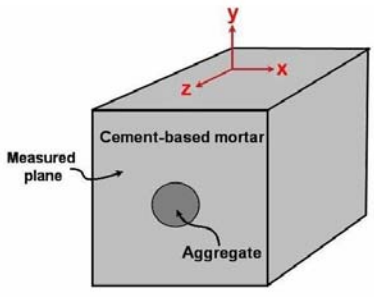

Figure 1 Specimen with the size of 50×50×50mm.

The cast specimens were then cured at room temperature (25°C) for 28 days before temperatures applied onto them. In this study, we investigate the micro-displacement of the specimens at six kinds of temperature degrees- 30°C, 50°C, 130°C, 230°C, 330°C and 420°C, respectively. Temperatures were applied by surrounding the specimens into a chamber of heater with heating rate of 2°C/min starting at room temperature. The investigated area of displacement is depicted in Fig.2.

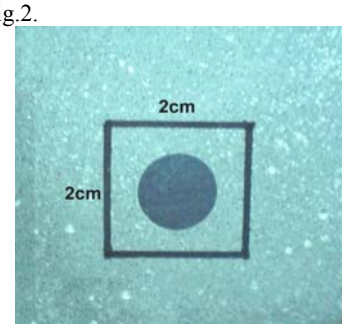

Figure 2 Investigated area (20×20mm).

2.2 ESPI measurements

The micro-displacement of the specimen was measured by ESPI with a wavelength of 532μm and precision of 25nm at various temperature degrees mentioned previously. The in-plane and out-of-plane displacement within the measured plane were both observed, where the displacement in x-y plane represents in-plane displacement, and in the z-direction is out-of-plane, as shown in Fig.1. The displacement of the specimen can be found by calculating speckle pattern observed by ESPI shown in Figs.3-4. The image converted from ESPI can display the displacement with 10nm per contour line. It should be mentioned that in Fig.3 and Fig.4, U-field interfere pattern was used to measure the in-plane displacement and W-field measures the out-of-plane displacement of the specimens.

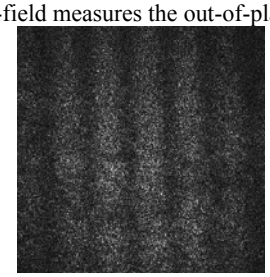

Figure 3 U-field interfere pattern.

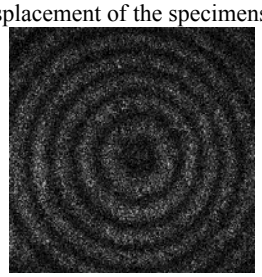

Figure 4 W-field interfere pattern.

Our experiments focus on observing the micro-displacement in a 20×20mm investigated area, particularly in the range of ITZ in between mortar matrix and single sand stone aggregate, as marked by T (top), B (bottom), L (left) and R (right) in Fig.5. The specific investigating positions, for example, at R point are d_0 (right on the

aggregate edge), d_1 (10μm away from d_0), and sequentially up to d_{12} (120μm away from d_0), as shown in Fig.6. The corresponding observed micro-displacements with respect to each observing position are denoted as δ_0, δ_1, δ_2…etc.

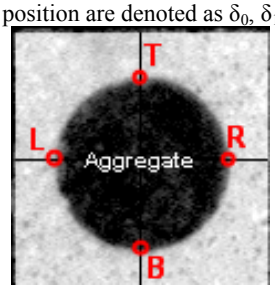

Figure 5 Measuring points.

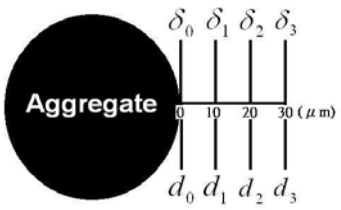

Figure 6 Observing position at R point.

3. RESULTS AND DISCUSSION

The displacement within ITZ caused by external temperature effects will change with respect to six designated temperatures, i.e. at 30°C, 50°C, 130°C, 230°C, 330°C and 420°C respectively. The displacement at each observing position around ITZ is measured by ESPI when the configured temperatures are reached. This kind of measurement is categorized as non-contact technique and can obtain the dynamic displacement of ITZ at various temperatures.

3.1 Displacement of ITZ

The displacements δ were measured at several discrete points from the edge of aggregate (d_0) to the anticipated edge of ITZ (d_{12}). The in-plane displacements (U-field) caused by temperature at T, B, L and R points (Fig.5), are summarized in Figs.7-10, respectively. As shown in Fig.7, the in-plane displacements on top of the aggregate (T point) decrease at 130°C and 330°C as the distance from the interface increases. In Fig.8, the behaviors of displacement over 230°C show no rational patterns due to dissipation of the bonding water within cement gel. The ITZ displacements at 30°C and 50°C increase with the temperature, and also slightly with the distance from the interface at top, left and right points of the aggregate, whereas decrease with the distance at bottom point. The caused ITZ displacements at L and R points (Figs.9-10) are very similar, especially at 130°C and 230°C the displacements reduce with the distance from the interface.

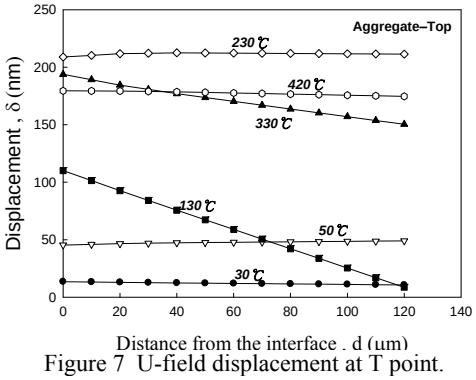

Figure 7 U-field displacement at T point.

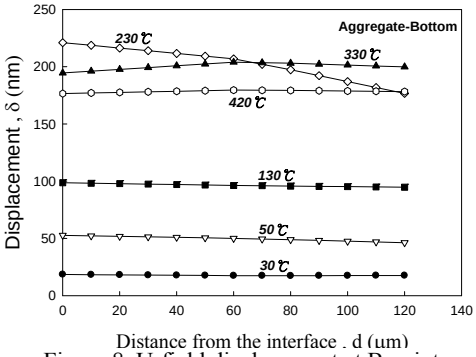

Figure 8 U-field displacement at B point.

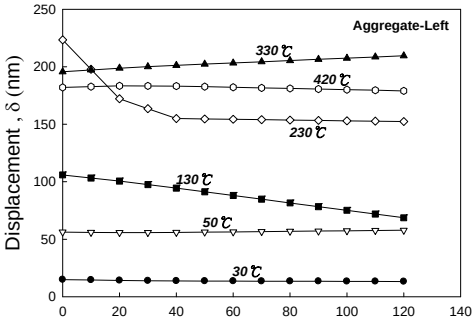

Figure 9 U-field displacement at L point.

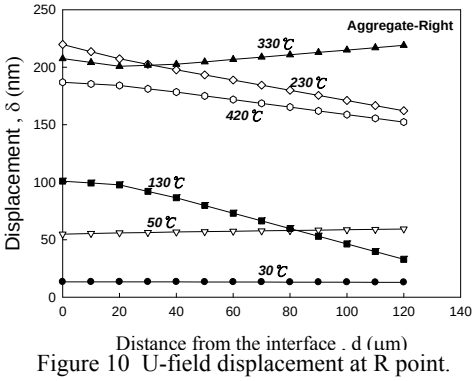

Figure 10 U-field displacement at R point.

The W-field (out-of-plane) displacements are shown in Figs.11-14. It can be observed that the temperature effects on ITZ micro-displacement are less prominent when the temperature goes beyond 130°C. Generally, the W-field displacement increases with temperature till 330°C at T point (Fig.11) and 230°C at the others (Figs.12-14). These trends are then reversed as the temperatures continue to increase. It appears that the changes of W-field displacement are more stable than of U-field with increasing temperatures. This may explain why the mortar (or binder) and the aggregate are easy to split each other since the thermal stress (the difference of the thermal strain) within ITZ in the radial direction is greater than that in the longitudinal direction. The results also suggest that the ITZ experiences certain inherent changes of material properties when temperature goes beyond 230°C.

3.2 Determination of ITZ

There are many measurement techniques such as SEM, OM, X-ray diffraction, micro-indentation and MIP to determine the range of ITZ. However, these methods can only observe an object with sizes that require sophisticated manufacturing processes. In addition, it is also challenging to maintain the object's original state of the interface when using these measurement techniques. As an alternative, we use ESPI technique here to determine the range of ITZ.

It is well recognized that the mechanical properties of ITZ are weaker than those of mortar (binder) and aggregates. Thereby, the displacement of ITZ is supposed to be sensitive to the applied temperatures that would alternate material's mechanical properties. From the results in Figs.7-14, we define a non-unit formula to calculate the difference of the displacement per unit distance:

$$\frac{\Delta\delta}{\Delta d} = \frac{\delta_{i+1} - \delta_i}{d_{i+1} - d_i} \tag{1}$$

The formula would give a constant value beyond ITZ due to homogeneous structure and thus can be used as a criterion to determine the range of ITZ.

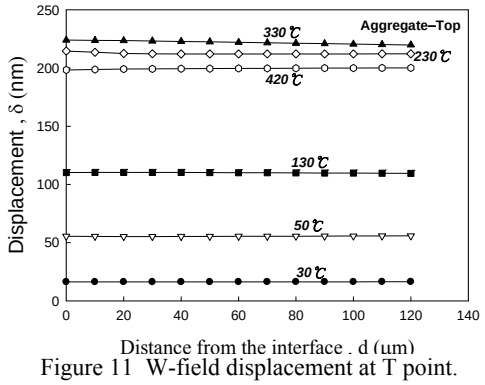

Figure 11 W-field displacement at T point.

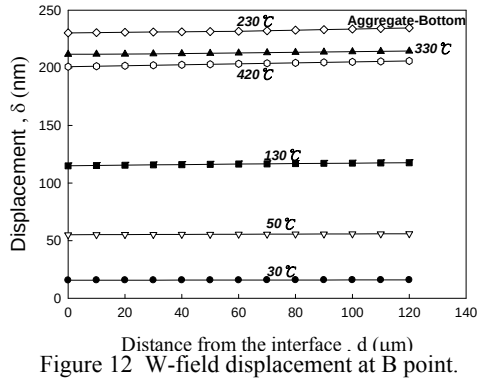

Figure 12 W-field displacement at B point.

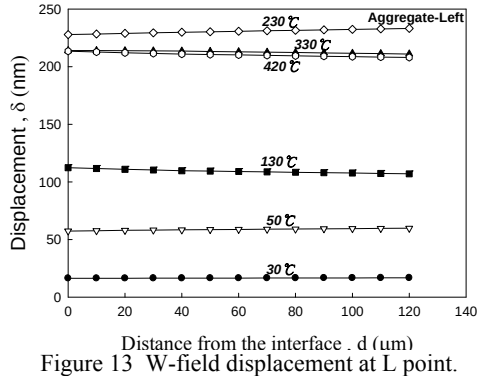

Figure 13 W-field displacement at L point.

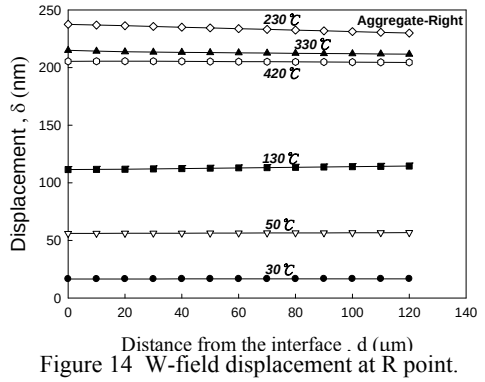

Figure 14 W-field displacement at R point.

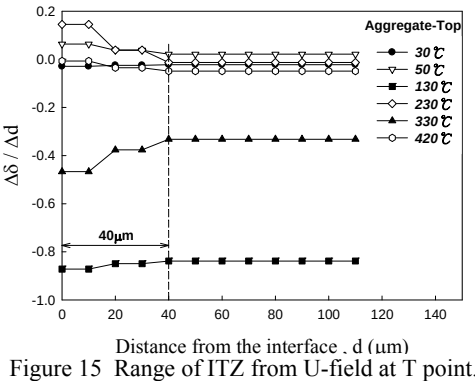

Figure 15 Range of ITZ from U-field at T point.

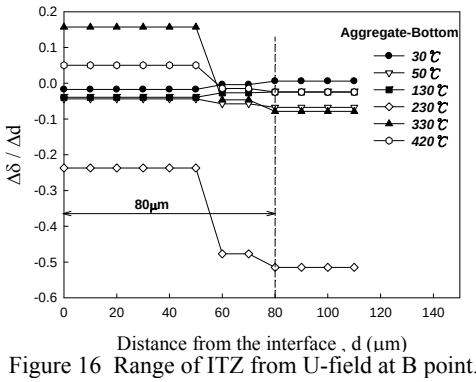

Figure 16 Range of ITZ from U-field at B point.

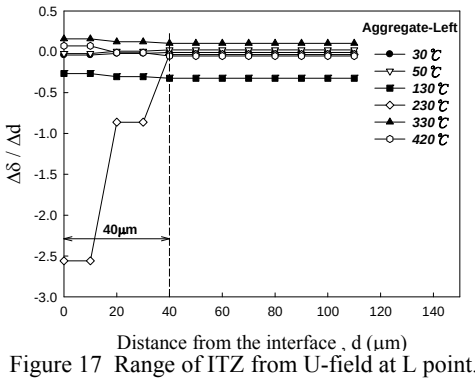

Figure 17 Range of ITZ from U-field at L point.

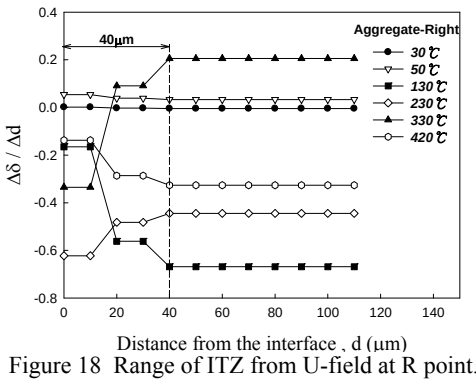

Figure 18 Range of ITZ from U-field at R point.

The ITZ determination results are depicted in Figs.15-18 (in-plane, U-field) and Figs.19-22 (out-of-plane, W-field), respectively. The range of ITZ is shown to be 40μm for the top, left and right points of the aggregate (Fig.15, 17-18), and 80μm for the bottom point (Fig.16). The calculation result is also supported by previous observations showing that the microstructure of ITZ at the bottom of aggregate is more porous comparing to other locations of the aggregate. We can also observe that the ITZ range of B point can be determined at room temperature. However, to more properly determine the ITZ of T, L and R points, the temperature should be increased to 130°C.

Figs.19-22 show the results of out-of-plane ITZ determination using W-field displacement. Similar to U-field, the ITZ range obtained from W-field is also 40μm at T, L and R points (Fig.19, 21-22). However, W-field ITZ at B point (Fig.20) appears to be 60μm, which is less than U-field ITZ (80μm). It can also be observed that at 50°C, the W-field ITZ determination for all the four points is sufficiently sensitive.

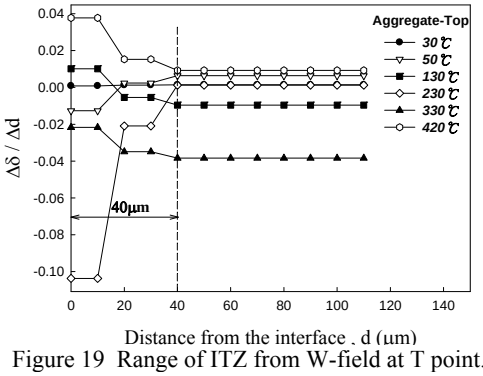

Figure 19 Range of ITZ from W-field at T point.

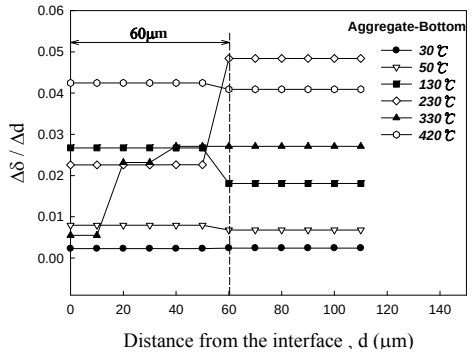

Figure 20 Range of ITZ from W-field at B point.

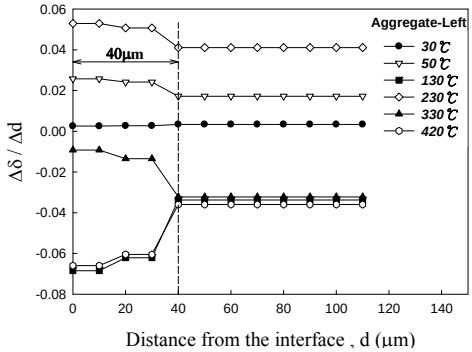

Figure 21 Range of ITZ from W-field at L point.

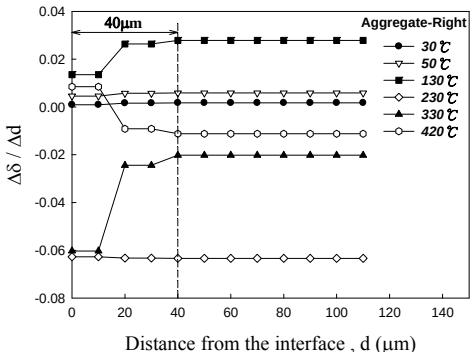

Figure 22 Range of ITZ from W-field at R point.

4. CONCLUSION

The micro-displacements of ITZ are investigated under six degrees of temperature (from room temperature to 420°C) using ESPI measurement technique. We conclude this study as follows.

(1) The maximum displacement of ITZ occurs at temperature 230°C to 330°C depending on the position around the aggregate. The temperature effects on both U-field and W-field ITZ displacement are similar at bottom, left and right points, but slightly different for top point.

(2) From the displacement observed by ESPI, material properties (displacement) of ITZ experience an inverse change at 230°C.

(3) The W-field ITZ displacements at all observing points are more stable to temperature changes than U-field ITZ displacements.

(4) The determined ITZ range at bottom point of the aggregate is 80μm for U-field observation, and 60μm for W-field observation, respectively. The ITZ ranges at top, left and right points of the aggregate are determined as 40μm in this study.

ACKNOWLEDGMENTS

This research was partially supported by the Taiwan National Science Council under Grant NSC 98-2221-E-151-054.

REFERENCES

[1] Mindess, S., "Tests to determine the mechanical properties of the interfacial zone", Interfacial Transition Zone in Concrete, Edited by J. C. Maso, 1996, pp47-48.

[2] Diamond, S., "Considerations in image analysis as applied to investigations of the ITZ in concrete", Cement Concrete Composites, 23, 2001, pp171-178.

[3] Liaoa, K. Y., Chang, P. K., Peng, Y. N. and Yang, C. C., "A study on characteristics of interfacial transition zone in concrete", Cement Concrete Research, 34, 2004, pp977-989.

[4] Zhang, J., Sun, H., Wan, J. and Yi, Z., "Study on microstructure and mechanical property of interfacial transition zone between limestone aggregate and Sialite paste", Construction Building Materials, 23, 2009, pp3393-3397.

[5] Diamond, S. and Huang, J., "The ITZ in concrete-a different view based on image analysis and SEM observations", Cement Concrete Composites, 23, 2001, pp179-188.

[6] Leemann, A., Loser, R. and Münch, B., "Influence of cement type on ITZ porosity and chloride resistance of self-compacting concrete", Cement Concrete Composites, 32, 2010, pp116-120.

[7] Elsharief, A., Cohen, M. D. and Olek, J., "Influence of aggregate size, water cement ratio and age on the microstructure of the interfacial transition zone", Cement Concrete Research, 33, 2003, pp1837–1849.

[8] Leemann, A., Münch, B., Gasser, P. and Holzer, L., "Influence of compaction on the interfacial transition zone and the permeability of concrete", Cement Concrete Research, 36, 2006, pp1425–1433.

[9] Cwirzen, A. and Penttala, V., "Aggregate–cement paste transition zone properties affecting the salt–frost damage of high-performance concretes", Cement Concrete Research, 35, 2005, pp671–679.

[10] Gao, J. M., Qian, C. X., "Liu, H. F. and Wang, B., Li, L., "ITZ microstructure of concrete containing GGBS", Cement Concrete Research, 35, 2005, pp1299-1304.

[11] Ollivier, J. P. and Maso, J. C., "Bourdette, B., Interfacial transition zone in concrete", Advanced Cement Based Materials, 2, 1995, pp30-38.

[12] Zhu, W. and Bartos, P. J. M., "Application of depth-sensing microindentation testing to study of interfacial transition zone in reinforced concrete", Cement Concrete Research, 30, 2000, pp1299-1304.

[13] Mouret, M., Bascoul, A. and Escadeillas, G, "Microstructural features of concrete in relation to initial temperature–SEM and ESEM characterization", Cement Concrete Research, 29, 1999, pp369-375.

[14] Fu, Y. F., Wong, Y. L., Poon, C. S., Chun-An Tang, C. A. and Lin, P., "Experimental study of micro/macro crack development and stress–strain relations of cement-based composite materials at elevated temperatures", Cement Concrete Research, 34, 2004, pp789-797.

[15] Wang, X. S., Wu, B. S. and Wang, Q. Y., "Online SEM investigation of microcrack characteristics of concretes at various temperatures", Cement Concrete Research, 35, 2005, pp1385-1390.